

Longitudinal variability of equatorial plasma bubbles observed by DMSP and ROCSAT-1

W. J. Burke

Space Vehicles Directorate, Air Force Research Laboratory, Hanscom Air Force Base, Massachusetts, USA

L. C. Gentile, C. Y. Huang, and C. E. Valladares

Institute for Scientific Research, Boston College, Chestnut Hill, Massachusetts, USA

S. Y. Su

Institute of Space Science, National Central University, Chung-Li, Taiwan

DISTRIBUTION STATEMENT A
Approved for Public Release
Distribution Unlimited

Received 11 May 2004; revised 2 July 2004; accepted 24 September 2004; published 4 December 2004.

[1] We compare observations of equatorial plasma bubbles (EPBs) by polar-orbiting satellites of the Defense Meteorological Satellite Program (DMSP) with plasma density measurements from the Republic of China Satellite (ROCSAT-1) in a low-inclination orbit. DMSP data were acquired in the evening sector at low magnetic latitudes between 1989 and 2002. ROCSAT-1 plasma densities were measured in March and April of 2000 and 2002. Observations of individual EPBs detected by both ROCSAT-1 and DMSP were well correlated when satellite orbital paths crossed the same longitude within approximately ± 15 min. We compiled a statistical database of ROCSAT-1 EPB occurrence rates sorted by magnetic local time (MLT), magnetic latitude, and geographic longitude. The rate of ROCSAT-1 EPB encounters at topside altitudes rose rapidly after 1930 MLT and peaked between 2000 and 2200 MLT, close to the orbital planes of DMSP F12, F14, and F15. EPB encounter rates have Gaussian distributions centered on the magnetic equator with half widths of $\sim 8^\circ$. Longitudinal distributions observed by ROCSAT-1 and DMSP are qualitatively similar, with both showing significantly fewer occurrences than expected near the west coast of South America. A chain of GPS receivers extending from Colombia to Chile measured a west-to-east gradient in S4 indices that independently confirms the existence of a steep longitudinal gradient in EPB occurrence rates. We suggest that precipitation of energetic particles from the inner radiation belt causes the dearth of EPBs. Enhancements in the postsunset ionospheric conductance near the South Atlantic Anomaly cause a decrease in growth rate for the generalized Rayleigh-Taylor instability. Results indicate substantial agreement between ROCSAT-1 and DMSP observations and provide new insights on EPB phenomenology. **INDEX TERMS:** 2415 Ionosphere: Equatorial ionosphere; 2439 Ionosphere: Ionospheric irregularities; 2435 Ionosphere: Ionospheric disturbances; 2455 Ionosphere: Particle precipitation; **KEYWORDS:** equatorial plasma bubbles, ionospheric scintillations, seasonal-longitudinal climatology, global ionosphere, South Atlantic Anomaly

Citation: Burke, W. J., L. C. Gentile, C. Y. Huang, C. E. Valladares, and S. Y. Su (2004), Longitudinal variability of equatorial plasma bubbles observed by DMSP and ROCSAT-1, *J. Geophys. Res.*, 109, A12301, doi:10.1029/2004JA010583.

1. Introduction

[2] The impending launch of the Communication/Navigation Outage Forecasting System (C/NOFS) satellite has sparked renewed interest in geophysical causes of equatorial spread F (ESF) and equatorial plasma bubbles (EPBs). Although both phenomena involve plasma density irregularities in the postsunset F layer that degrade electromagnetic signal propagation, they are not identical. The term ESF describes irregular signatures on ionograms due to backscatter from and above the bottomside of the nighttime

F layer. The term EPB refers to irregular plasma density depletions observed by satellites and radar backscatter [Woodman and LaHoz, 1976] in the topside ionosphere. Because of their appearance in altitude-versus-time radar displays and ionograms, EPBs are also referred to as plasma plumes [Woodman and LaHoz, 1976] and range spread F [Aarons, 1993]. Radar measurements taken during an Atmosphere Explorer E (AE-E) overflight of Kwajalein show that plumes/bubbles have elongated, wedge-like cross sections that extend from their bottomside sources into the topside ionosphere [Tsunoda *et al.*, 1982].

[3] Both ESF and EPBs begin as generalized Rayleigh-Taylor (R-T) instabilities [Ott, 1978] in the bottomside of the F layer. EPBs are nonlinear evolutions of the R-T

instability in which bottomside plasma interchanges with plasma near and above the F layer peak. Severe radio signal degradation occurs at off-equatorial latitudes when irregular plasma within density depletions propagates into the topside ionosphere. A basic understanding of ESF/EPB causality is obtained by considering the linear growth rate γ of the generalized R-T instability and the geophysical contexts in which it is realized. *Haerendel* [1973] pointed out that flux-tube integrated Pedersen conductances, Σ_P , control the magnitude of γ rather than local conductivity near the apex of magnetic field lines threading the bottomside of the F layer. *Ott* [1978] showed that zonal electric fields also influence R-T growth rates. Eastward/westward fields enhance/quench growth. We chose a local system of coordinates with X positive toward magnetic east, Y positive along the magnetic field \mathbf{B} , and Z perpendicular to \mathbf{B} and positive in the vertically upward direction. Adopted to this coordinate system, a formulation derived by *Sultan* [1996] captures both effects:

$$\gamma = \frac{\Sigma_P^F}{\Sigma_P^E + \Sigma_P^F} \left(V_p - U_n^P - \frac{g_L}{\nu_{in}^{eff}} \right) \frac{1}{L_n} - R_T, \quad (1)$$

where g_L represents the downward acceleration due to gravity, $V_p = \mathbf{E} \times \mathbf{B}/B^2$ is the vertical component of plasma drift due to the zonal component of the electric field \mathbf{E} at the magnetic equator, U_n^P is the vertical component of neutral wind velocity perpendicular to \mathbf{B} , and ν_{in}^{eff} is the effective, flux-tube integrated, F region, ion neutral collision frequency weighted by number density in the flux tube. L_n is the scale length of the vertical gradient of the flux-tube integrated plasma density measured at the equator. R_T is the flux-tube integrated recombination rate [*Basu*, 1997]. Σ_P^E and Σ_P^F are the contributions to Σ_P from the E and F regions, respectively. In the bottomside of the F layer in the postsunset ionosphere, L_n is positive. Positive contributions to γ derive from eastward components of \mathbf{E} and downward components of U_n^P . Under typical ionospheric conditions growth periods, $1/\gamma$, are ~ 10 min. It takes several growth periods for large-amplitude irregularities to grow. Since \mathbf{g} and \mathbf{B} are constants at a given location, R-T growth rates are controlled by the variability of E_0 , U_n^P , Σ_P^E , Σ_P^F , ν_{in}^{eff} , R_T , and through the flux-tube integrated quantities by the height of the F layer.

[4] Eastward electric fields in the dusk sector have three sources: (1) leakage of the solar quiet (S_q) current system into the nightside ionosphere [*Eccles*, 1998a, 1998b], (2) penetration electric fields from high to low latitudes [*Nopper and Carovillano*, 1978; *Fejer and Scherliess*, 1997], and (3) tropospheric gravity waves [*Hysell et al.*, 1990; *Singh et al.*, 1997; *McClure et al.*, 1998]. S_q current sources act systematically, while penetration electric field events are episodic. Gravity wave seeding seems to occur both episodically [*Singh et al.*, 1997] and regionally [*Meriwether et al.*, 1996]. Most systematic measurements of eastward electric fields reported to date come by way of inference from vertical plasma flows observed by the ion drift meter experiments on satellites such as AE-E and the Republic of China Satellite (ROCSAT-1). Electric field models have been derived from measurements of the incoherent backscatter radar at Jicamarca in Peru [*Scherliess*

and *Fejer*, 1999]. In general, vertical plasma drifts near the dusk terminator are characterized by prereversal enhancements [*Fejer et al.*, 1991]. In the early evening local time (LT) sector, plasma initially rises as polarization charges develop near the terminator. After ~ 2000 LT the direction of the vertical plasma drift usually reverses to stabilize the bottomside of the F layer against irregularity formation. In this scenario a finite window of opportunity is available after sunset for EPBs to form before damping forces become dominant. The intensities of prereversal enhancements in vertical drift are subject to seasonal, longitudinal, and solar cycle variability. For future reference, we note that vertical drifts observed at Jicamarca tend to be largest near the equinoxes of solar maximum years [*Scherliess and Fejer*, 1999].

[5] Equation (1) indicates that the R-T growth rate is inversely proportional to Σ_P^E . *Stephan et al.* [2002] demonstrated that sporadic E layers can reduce γ by a factor of two. EPBs should grow most rapidly at longitudes where zonal gradients of Σ_P at the dusk meridian are strongest. Conversely, the equatorial ionosphere is stable if one foot of a field line remains in sunlight for some time after the conjugate E region enters darkness. *Tsunoda* [1985] argued that the steepest gradients in Σ_P^E occur where magnetic flux tubes closely align with the terminator. Thus the observed seasonal versus longitudinal (S/L) variability of range spread F and severe radio signal scintillation is largely controlled by magnetic declination δ . At longitudes where $\delta \approx 0^\circ$, EPB formation is favored near the equinoxes. In regions of strong westward (eastward) δ , the minimum angle between flux tubes and the dusk terminator shifts toward the December (June) solstice. *Aarons* [1993] and *Huang et al.* [2001, 2002] demonstrated that the general features of *Tsunoda's* prescription for S/L variations are replicated in global EPB occurrence rates.

[6] *Burke et al.* [2004] examined latitudinal plasma density profiles in the evening sector measured between 1989 and 2000 during $>75,000$ orbits of Defense Meteorological Satellite Program (DMSP) satellites. A DMSP satellite encountered one or more EPBs during >8300 orbits. This large database proved sufficient to test *Tsunoda's* hypothesis on a monthly rather than seasonal scale. Each data bin (1 month in duration and 15° wide in longitude) contained ~ 260 samples, assuring statistical significance. The angle α between δ and the terminator line is independent of time in the solar cycle. DMSP observations generally support *Tsunoda's* hypothesis, in that the maximum rates of EPB detection occurred near days when $\alpha = 0^\circ$. However, unpredicted and systematic offsets from $\alpha = 0^\circ$ days occurred in many longitude sectors. In most sectors occurrence rates were not symmetric with respect to the two times per year when the magnetic field aligned with the dusk terminator. Some of the phase offsets and asymmetries probably reflect EPB suppression due to interhemispheric winds [*Mendillo et al.*, 1992; *Kil and Heelis*, 1998].

[7] Longitudinal differences that the *Tsunoda* model does not attempt to explain appear in the EPB occurrence rates. For example, in all years of the solar cycle, EPBs occurred more often in the Atlantic-African than in the Pacific sector. *Huang et al.* [2001] suggested that for a given eastward electric field in the dusk sector, $V_p \propto E/B$ is largest where the magnetic field B is weakest. For this reason R-T

irregularities should grow fastest at longitudes where the Earth's magnetic field at the equator is weakest. As discussed below, nature is more complex than this conjecture supposes.

[8] Questions remain regarding the comprehensiveness of EPB detections by DMSP and their relation to radiowave scintillations observed on the ground. To begin answering these questions, *Burke et al.* [2003] compared a subset of EPB detections by DMSP with radar plumes and intense ultrahigh frequency (UHF) scintillation episodes observed at Jicamarca and Ancon, Peru. Again, the seasonal variabilities of EPBs, radar plumes, and intense scintillations were similar. Combined ground and satellite observations also suggest that plasma bubbles tend to form in bursts rather than as isolated events. Despite the obvious limitations of using polar-orbiting satellites to monitor equatorial electrodynamics, DMSP yields a credible global climatology of EPB occurrence. The DMSP database offers an opportunity to perform statistical tests of proposed hypotheses on a global scale.

[9] This paper continues to test the comprehensiveness of EPB detections by DMSP through comparisons with plasma density observations from ROCSAT-1 in the evening sector. The ROCSAT-1 data used in our study were acquired during March and April of 2000 and 2002. In the year 2000 (2002), four (three) DMSP satellites were flying in the postsunset LT sector. Our analysis includes direct comparisons both of individual EPB observations and their global distributions. Because the South American sector is the most highly instrumented region of the world for making comprehensive measurements of equatorial ionosphere/thermosphere dynamics [*Basu et al.*, 1996; *Groves et al.*, 1997; *Pimenta et al.*, 2003; *Valladares et al.*, 2004a], it is a major resource for the C/NOFS mission. For this reason we pay special attention to satellite data acquired at eastern Pacific and South American longitudes. Our observations indicate that contrary to the conjecture of *Huang et al.* [2001], systematic effects, unique to this longitude sector, act to lower rather than raise rates of EPB occurrence. We suggest that electrons in the drift loss cone [*Torr et al.*, 1975; *Luhmann and Vampola*, 1977; *Blake et al.*, 2001] precipitate from the radiation belt and increase Σ_E at the southern ends of magnetic field lines near the Appleton anomaly crest. This effect slows but does not inhibit the linear growth of bottomside spread F at these longitudes. However, it appears to provide conducting paths to bleed polarization charges from the walls of bubbles as they evolve nonlinearly into the topside ionosphere [*Ott*, 1978].

[10] Because of the very different orbital inclinations of the DMSP and ROCSAT-1 satellites, care must be exercised to make meaningful comparisons between their measurements. The following section briefly describes their similar measurement capabilities and the opportunities/restrictions imposed by their different orbital inclinations. The observations section first summarizes the low-latitude plasma density database of DMSP EPB encounters accumulated over a 13-year period. We next compare observations of an EPB detected by both ROCSAT-1 and DMSP and then demonstrate an empirical pattern recognition method for automatically identifying bubbles in the ROCSAT-1 data stream. The latter allows us to specify EPB occurrence rates observed by ROCSAT-1 as functions of magnetic local time

(MLT), magnetic latitude (MLat), and geographic longitude (GLon). Finally, we compare satellite crossings of EPBs with several L-band scintillations observed in western South America during March and April 2002. The discussion section examines some implications of the data set comparisons, especially the appearance of the unexpected influence of precipitation from the inner radiation belt on EPB occurrence in the eastern Pacific and South American longitude sectors. Higher scintillation rates were detected along a chain of GPS receivers in South America while looking to the east rather than to the west [*Valladares et al.*, 2004b]. These observations are consistent with a steep zonal gradient in EPB occurrence inferred from satellite data.

2. Sensor and Orbital Considerations

[11] DMSP satellites are three-axis stabilized spacecraft that fly in circular, Sun-synchronous polar orbits (inclination 98.7°) at an altitude of ~ 840 km. The orbital planes are near either the 1800–0600 or 2100–0900 geographic LT meridians with the ascending nodes on the duskside of the Earth. Each satellite carries a suite of sensors called the Special Sensor Ions, Electrons, and Scintillation (SSIES) to measure the densities, temperatures, and drift motions of ionospheric ions and electrons. SSIES consists of a spherical Langmuir probe mounted on an 0.8 m boom to measure the densities and temperatures of ambient electrons, along with three separate sensors mounted on a conducting plate facing in the ram direction [*Rich and Hairston*, 1994]. These are (1) an ion trap to measure the total ion density, (2) an ion drift meter to measure horizontal (V_H) and vertical (V_V) cross-track components of plasma drifts, and (3) a retarding potential analyzer to measure ion temperatures and in-track components of plasma drift V_{\parallel} .

[12] Orbital periods of DMSP satellites of ~ 104 min allow an average of 14 orbits per day. Between orbital ascending nodes, DMSP satellites regress $\sim 25^\circ$ in longitude. Following *Huang et al.* [2002], we first divide the DMSP data into 24 longitude bins each 15° in width. We normalize results as the rate of EPB encounters defined by the ratio of the number of orbits in which at least one EPB was detected divided by the number of orbits in the longitude bin. During the course of a month a DMSP satellite revisits each longitude sector ~ 18 times. During every orbit DMSP satellites twice sample all magnetic latitudes in the $\pm 40^\circ$ MLat band within narrowly specified ranges of local time.

[13] ROCSAT-1 was launched on 27 January 1999, into a circular orbit at an altitude of 600 km and an inclination of 35° . In this configuration the orbit's ascending node precesses westward at a rate of $\sim 7^\circ$ per day. The scientific payload includes an Ionospheric Plasma and Electrodynamics Instrument (IPEI) that is similar to SSIES and consists of an ion trap, two drift meters, and a retarding potential analyzer [*Yeh et al.*, 1999]. The full electrodynamics capabilities of IPEI have been used to analyze detailed characteristics of individual EPBs [*Yeh et al.*, 2001; *Chen et al.*, 2001]. This current study concentrates on the global distribution of EPBs found in 1-s averaged plasma densities acquired in the evening (1800 to 2400) MLT sector during March and April of the years 2000 and 2002.

[14] With an orbital period of ~ 96 min, ROCSAT-1's ascending node regresses 24° to the west from one orbit to the next. This period allows an average of 15 (450) orbits per day (month). Because of ROCSAT-1's orbital period and inclination, it typically samples plasma densities within a given longitude sector at evening local times three to four times per day. However, the MLat range sampled in the evening sector varies widely from one week to the next. Periods of continuous magnetic equatorial crossings are followed by intervals in which the entire evening sector pass is spent poleward of the Appleton anomaly crests.

[15] A chain of ten Global Positioning System (GPS) receivers has been installed in western South America to monitor the variability of total electron content (TEC) and L-band scintillations [Valladares *et al.*, 2004a]. The chain extends from Bogota, Colombia, to Antuco, Chile, near the 286°E meridian. A simple technique was developed to demonstrate the day-to-day variability in intensity and MLat of the S4 index at GPS frequencies. By definition, the S4 index measures the ratio of the standard deviation in the intensity of a carrier frequency divided by its mean value. Intervals of high values of S4 frequently correspond to times when a plasma bubble intersects the receiver's field of view. We use data acquired by the GPS receiver chain during March and April 2002 to validate and interpret ROCSAT-1 and DMSP observations during this 2-month interval.

3. Observations

[16] This section treats three related topics. We first present an overview of plasma density depletions observed by DMSP satellites at low latitudes in the evening (19.25–21.5 MLT) sector from 1989 to 2002. Second, we consider an example of a plasma bubble encountered by ROCSAT-1 and two DMSP satellites. This leads to an automated procedure for identifying plasma bubbles in ROCSAT-1 data streams. Third, we demonstrate how orbital characteristics influenced ROCSAT-1 opportunities to encounter EPBs acquired in March and April of 2000 and 2002.

[17] Several methods of comparing ROCSAT-1 and DMSP measurements are possible. In crossing the evening MLT sector during a given orbit, ROCSAT-1 samples $\sim 90^\circ$ in longitude within a limited MLat range. The LT planes of DMSP orbits are fixed. Thus DMSP satellites cover limited spans of longitude while flying between $\pm 30^\circ$ MLat. Huang *et al.* [2001] opted to develop DMSP statistics on a very simple basis: did a DMSP satellite cross at least one bubble during a given evening sector pass? Statistics were based on the ratio of orbits with bubbles divided by the total number of orbits within each 15° longitude bin. This simple criterion could be applied to ROCSAT-1 as well. In March and April 2000 ROCSAT-1 detected EPB signatures in 297 out of ~ 900 orbits, while DMSP F11 (~ 1918 MLT), F12 (~ 2012 MLT), F14 (2030 MLT), and F15 (~ 2112 MLT) detected EPBs during 37, 238, 268, and 276 out of ~ 840 orbits. These numbers indicate little more than the facts that ROCSAT-1 and DMSP detected EPBs at comparable rates and a strong MLT gradient in EPB occurrence occurs at topside altitudes.

[18] Much more information about EPB distributions can be garnered from ROCSAT-1 data. In the analysis presented

below we divide the data into 15° bins in GLon, 5° in MLat, and 0.5 hours in MLT. Statistics are presented as ratios of time spent in EPBs divided by the total time spent within individual bins. Criteria for identifying EPB encounters in ROCSAT-1 data are discussed below. Longitudinal distributions detected by ROCSAT-1 are compared with those accumulated by DMSP satellites during the same 2 months but over a 13-year period. Steep gradients in the rates of EPB detections found in both satellite data sets over South America are shown to be consistent with observations from the GPS receiver network [Valladares *et al.*, 2004b].

[19] Figure 1 shows a rate of occurrence map for EPBs observed by DMSP satellites plotted on a month-versus-longitude grid. As indicated above, occurrence rates were calculated as simple ratios of the number of orbits in which EPBs were detected divided by the total number of orbits in each month/GLon bin. The rates are represented by the designated color codes. Over 13 years, DMSP satellites sampled each bin more than 300 times. We recorded neither the total time DMSP satellites spent within bubbles nor whether multiple EPB encounters occurred in a given pass. Dark lines on the map indicate the days when α , the angle between equatorial declination δ and the dusk terminator, was zero. The seasonal-longitudinal model of Tsunoda [1985] predicts that EPB occurrence rates should peak near times when $\alpha = 0^\circ$. Figure 1 extends a similar map in the work of Burke *et al.* [2004] with the addition of the 2 solar maximum years 2001 and 2002. Data for the months of March and April form the basis for comparison with ROCSAT-1 measurements.

[20] Figure 2 shows the northeasterly trajectory of ROCSAT-1 from 1303 to 1321 UT on 2 March 2000. The data were acquired in the evening sector (1800–2400 MLT) as the spacecraft flew from the Indian Ocean toward the western Pacific Ocean. We have compared ROCSAT-1 observations with ion density measurements from four DMSP satellites F11, F12, F14, and F15 whose orbits cross the magnetic equator near 1915, 2015, 2030, and 2106 MLT, respectively. F11 and F14 (F12 and F15) intersected ROCSAT-1's trajectory near 100° (115°) E at 1249 and 1357 (1249 and 1330) UT, respectively. Plasma densities measured by ROCSAT-1 during this interval are plotted as functions of UT, GLon, MLat, and MLT in Figure 3. Between 1314:24 and 1315:16 UT, ROCSAT-1 crossed a structure, centered near 115°E , in which the density decreased from 10^6 to $7 \times 10^4 \text{ cm}^{-3}$. Figure 4 shows the density profiles measured during the DMSP F12 and F15 passes of Figure 2. Between 1250 and 1254 UT F12 encountered a highly irregular depletion in which the density fell from $\sim 3 \times 10^5$ to a minimum of $9 \times 10^4 \text{ cm}^{-3}$. F15 detected a similar depletion between 1328 and 1336 UT, probably the same EPB. Near the magnetic equator at $\sim 100^\circ\text{E}$, ROCSAT-1, DMSP F11, and F14 did not detect EPB signatures.

[21] To establish a statistical database for comparison with DMSP measurements summarized in Figure 1, we developed a pattern recognition algorithm to automate the identification of EPBs in ROCSAT-1 data. By trial and error, we found that by setting a threshold change in the $|\Delta \log N| > 0.015$ from one second to the next we were able to trace EPBs in the plasma density profiles. Figure 5 illustrates a sample result of this selection process. Red

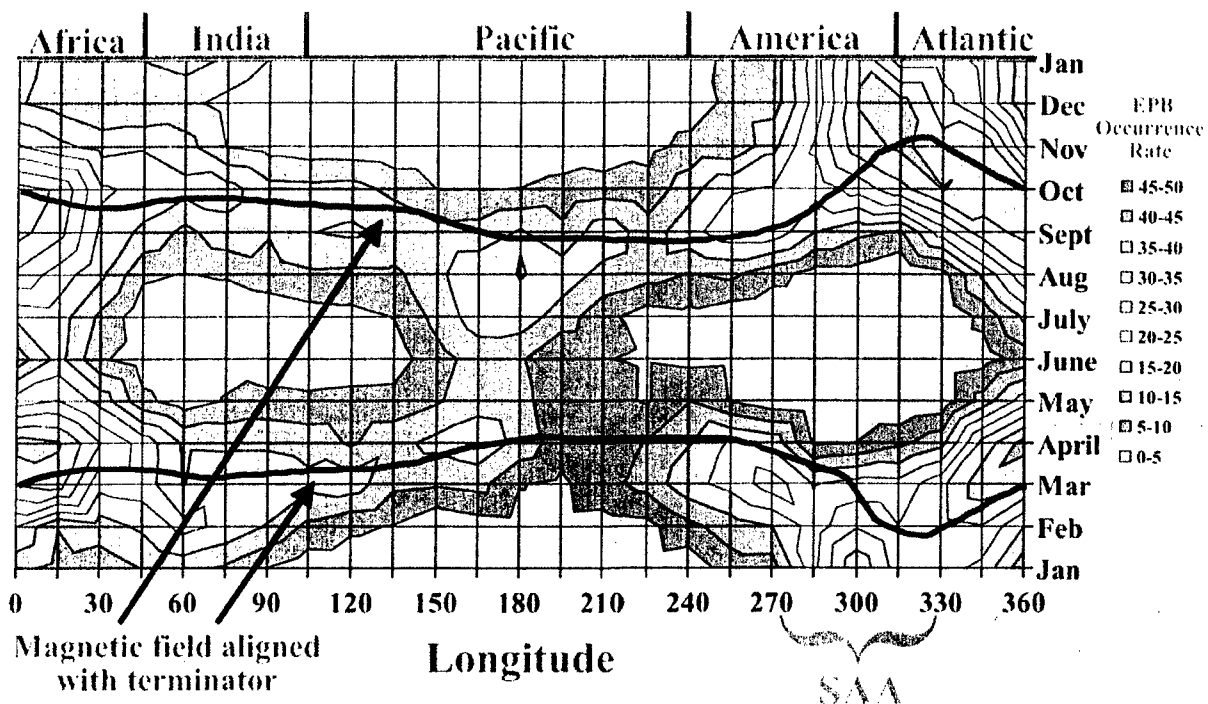


Figure 1. Contours of equatorial plasma bubble (EPB) occurrence rates measured by DMSP satellites between 1989 and 2002 plotted on a month versus longitude grid in nine 5% increments. The solid lines indicate the two times per year when $\alpha = 0^\circ$ at given longitudes. See color version of this figure at back of this issue.

triangles indicate time spent inside EPBs; regions outside of bubbles were not selected. Choosing thresholds $|\Delta \log N| < 0.01$ led to the selection of small density fluctuations not associated with EPBs. Conversely, a threshold $|\Delta \log N| > 0.02$ resulted in missing interior portions of bubbles. With this criterion we calculated the time spent within EPBs for each MLT, MLat, and GLon bin. Consistent with the conjecture of *Burke et al.* [2003], ROCSAT-1 detected many more multiple (Figure 5) than single (Figure 3) bubble structures during individual low-latitude passes through the evening ionosphere.

[22] We have compared all ROCSAT-1 orbits in March and April 2000 during which EPBs were detected with plasma density measurements taken by DMSP F11, F12, F14, and F15 at low latitudes in the evening sector during the same period. In general, if their trajectories crossed within approximately ± 15 min, both ROCSAT-1 and DMSP measured quiescent or disturbed plasma densities. The few exceptions were depletions observed by ROCSAT-1 but not by DMSP very close to the magnetic equator. Such cases suggest that the bubbles had floated to an altitude greater than 600 km but less than 840 km at the times of the satellite passes.

[23] On many days DMSP satellites detected EPBs while ROCSAT-1 did not. As illustrated in Figures 6 and 7, this is a sampling artifact of the ROCSAT-1 orbit. The top plot of each figure shows the magnetic latitude at which ROCSAT-1 crossed the 2100 MLT meridian between 1 March and 30 April. The MLat range for a given day reflects variations of the magnetic equator with geographic longitude. Since the

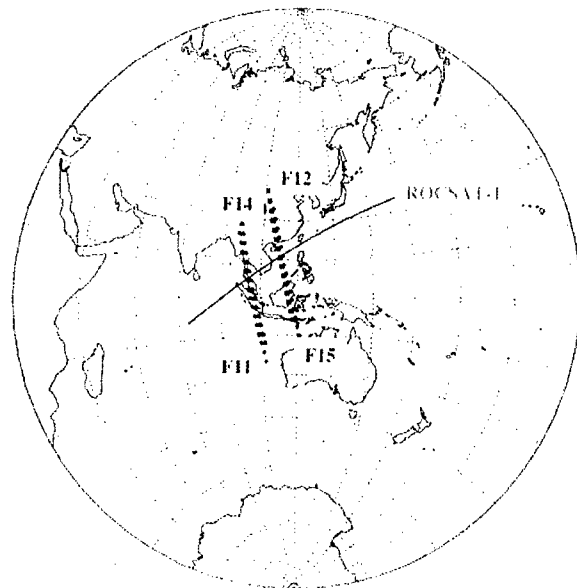


Figure 2. Trajectory of ROCSAT-1 in the evening MLT sector between 1303 and 1321 UT on 2 March 2000 along with near-in-time crossing trajectories of four DMSP satellites.

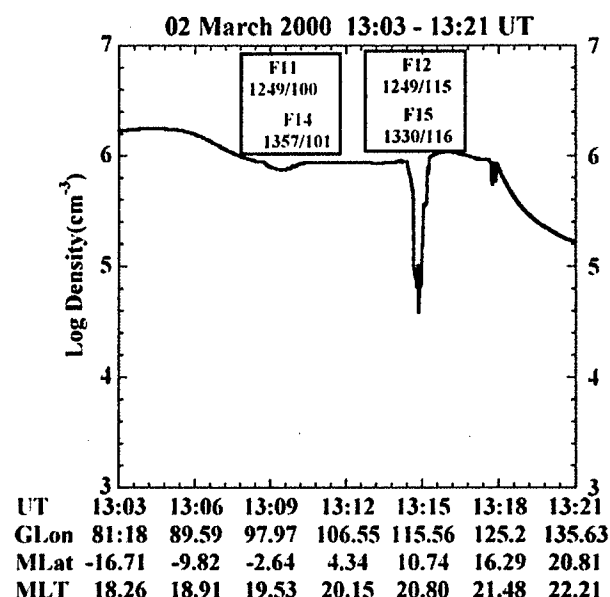


Figure 3. Plasma densities measured by ROCSAT-1 along the trajectory shown in Figure 2. The UT and geographic longitude at which the four DMSP trajectories crossed that of ROCSAT-1 are indicated. DMSP F12 and F15 detected EPBs at approximately the same longitude (115°E) as the density depletion crossed by ROCSAT-1.

ROCSAT-1 orbital plane precesses $\sim 7^\circ$ per day, a similar distribution of points, advanced/delayed by 2 days, represents MLat locations of the satellite near the 2200/2000 MLT meridians. The 2100 MLT meridian was chosen for display

because it is close to the orbital plane of F15, the DMSP satellite that detected the most EPBs. The bottom plots of Figures 6 and 7 show the percentage of time that ROCSAT-1 detected EPBs in a given longitude bin as a function of day in March and April 2000 and 2002, respectively. The displays are similar to that used in Figure 1 but with the longitude-day axes interchanged. Note that ROCSAT-1 data are unavailable for 14 March 2002 (Julian day 73) and are limited for 26 April 2000 (day 117).

[24] Data plotted in Figures 6 and 7 show that in both years ROCSAT-1 went through alternating periods when it detected EPBs in almost all/no orbits. Roughly, the days with/without EPB encounters correspond to times when evening sector orbits were equatorward/poleward of 20° MLat. We note that ROCSAT-1 detected some EPBs during orbits that crossed the 2100 MLT meridian at magnetic latitudes poleward of 20° (e.g., days 73–77, 2000). Almost invariably, these EPB detections occurred in the 2200–2400 MLT sector when ROCSAT-1 was at magnetic latitudes equatorward of 20° . Quantitative distributions of EPB encounters by ROCSAT-1 as a function of MLat are given below.

[25] Figure 8 shows EPB occurrence rates plotted as a function of MLT. The figure also indicates the MLT meridians where the four DMSP satellites crossed the magnetic equator. Three empirical points should be noted. First, occurrence rates were similar in the 2 years. This is consistent with measurements from the DMSP F14 and F15 satellites that detected EPBs in 17.7% and 18.5% of their 2000 and 2002 orbits, respectively. Second, between 1930 and 2000 MLT the occurrence rates rose to sustained high levels in both years. Consistent with this result, while it was still operating in 2000, F11 seldom detected EPBs near 1915 MLT. The orbital planes of DMSP F12, F14, and F15

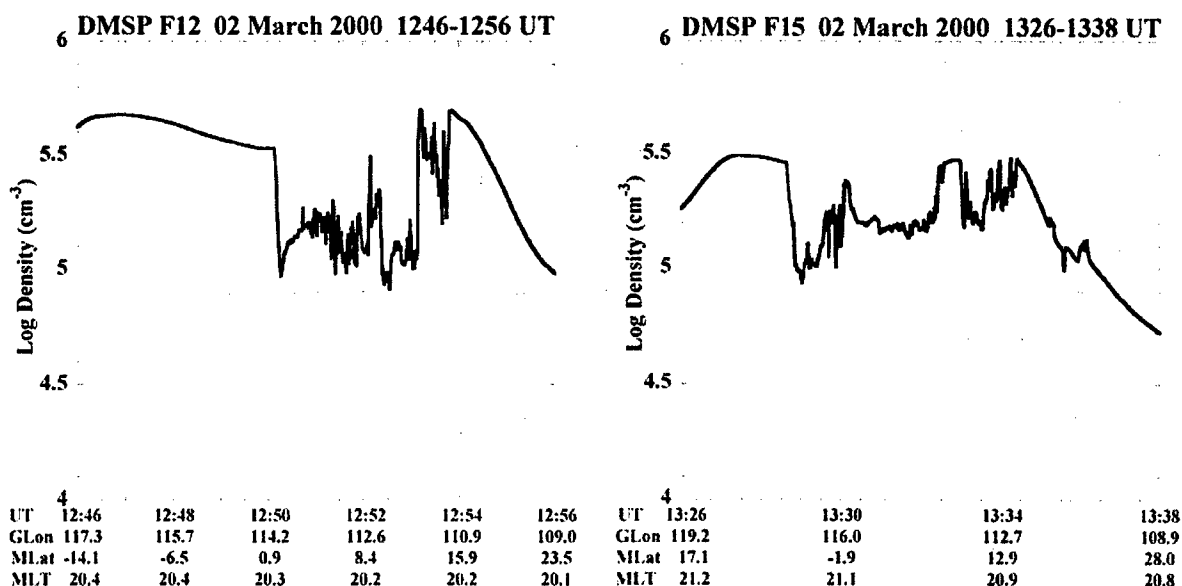


Figure 4. Plasma densities measured on 2 March 2000 by DMSP F12 between 1246 and 1256 UT (left) and by DMSP F15 between 1326 and 1338 UT (right). In both cases, the deep depletions were observed at approximately the same longitude (115°E) as the EPB that ROCSAT-1 encountered (Figure 3).

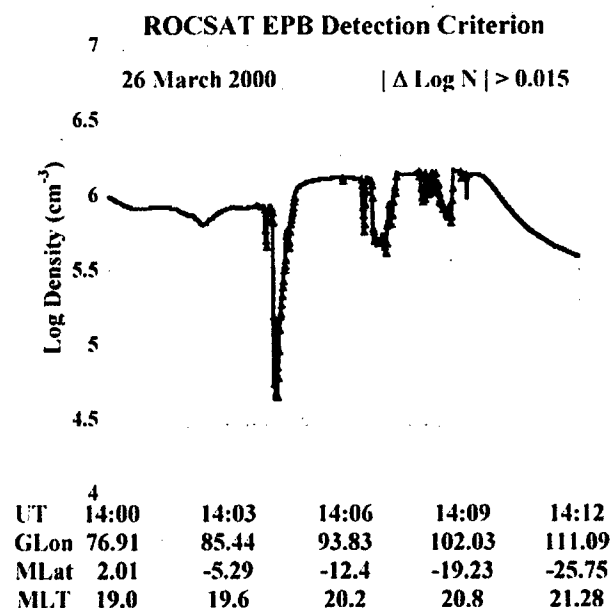


Figure 5. Example of automatic bubble selection criterion for the ROCSAT-1 1-s plasma density data with $|\Delta \text{Log } N| > 0.015$. Triangles indicate the time spent inside EPBs. Cumulative time spent in EPBs was used to determine statistical distributions of EPB occurrence by longitude, MLat, and MLT.

are in the MLT sector where ROCSAT-1 recorded the highest EPB occurrence rates. Third, ROCSAT-1 detected EPBs, albeit at slightly lower rates, in the late evening sector not sampled by DMSP.

[26] Figure 9 plots ROCSAT-1 occurrence rates in March and April 2000 and 2002 as functions of magnetic latitude. As indicated, data from the two years have similar Gaussian-like distributions centered at the magnetic equator, with $\sigma \approx 8^\circ$. Thus ROCSAT-1 detected $>90\%$ of the EPB density depletions within $\pm 16^\circ$ of the magnetic equator.

[27] Figure 10 compares EPB occurrence rates observed by DMSP and ROCSAT-1 as a function of geographic longitude. The top plot of Figure 10 shows B_{eq} , the intensity of the Earth's field at the magnetic equator at an altitude of 350 km, which ranges between 3.4×10^4 and 2.2×10^4 nT at $\sim 100^\circ$ and 300° E, respectively. The second and third plots show EPB occurrence rates detected by ROCSAT-1 in March and April 2000 and 2002 and by DMSP satellites in March and April 1989–2002, respectively. The dashed line in the ROCSAT-1 plot gives the average value for the 2 years in each longitude bin. The solid line in the DMSP plot represents a polynomial fit to March and April data extracted from Figure 1. In both instances the lines are meant as guides for the eye to which we attribute no physical significance. Attention is directed to two empirical facts. First, the occurrence rate-versus-longitude distributions seen by ROCSAT-1 and DMSP during March and April appear quite similar in shape. The correlation coefficient between

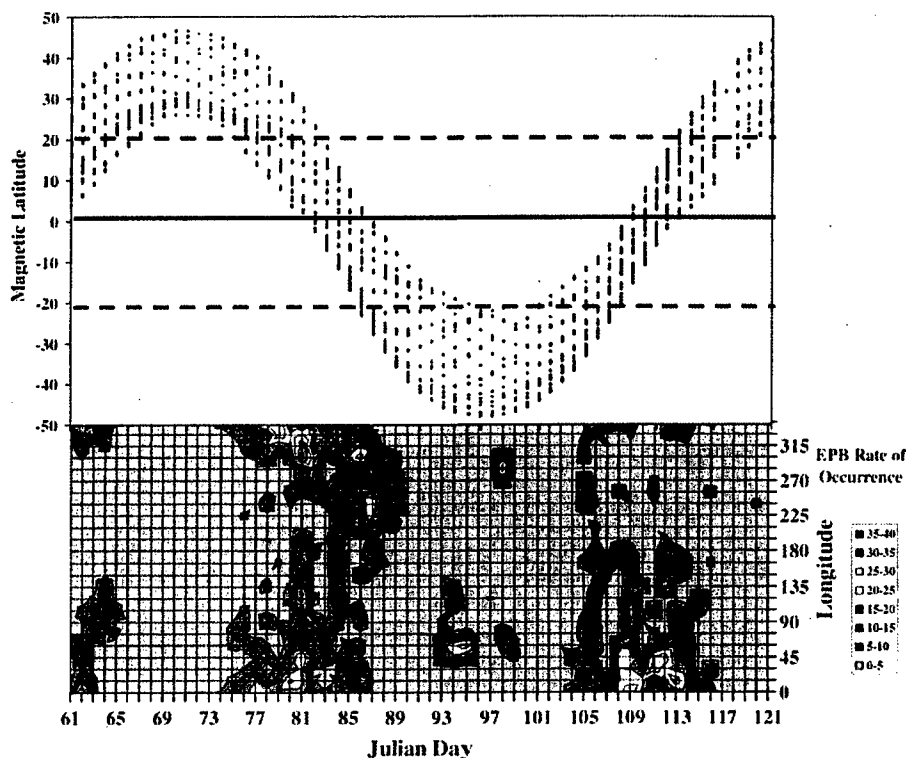


Figure 6. Magnetic latitudes of ROCSAT-1 at 2100 MLT (top) and contours of EPB occurrence rates plotted on a longitude versus Julian day grid (bottom) for 1 March to 30 April 2000. See color version of this figure at back of this issue.

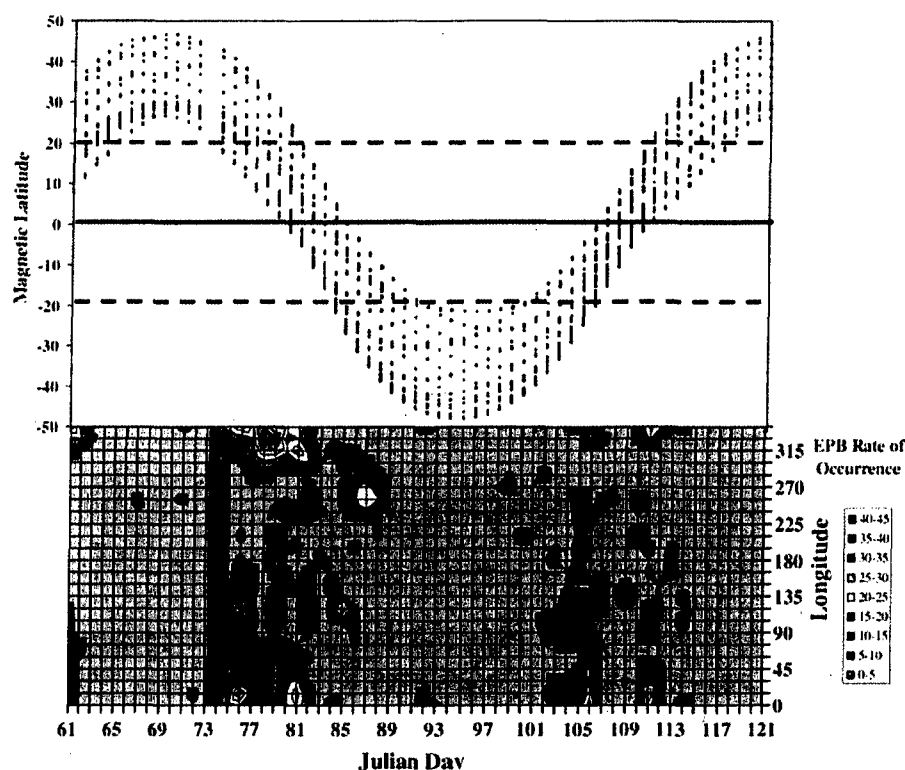


Figure 7. Magnetic latitudes of ROCSAT-1 at 2100 MLT (top) and contours of EPB occurrence rates plotted on a longitude versus Julian day grid (bottom) for 1 March to 30 April 2002. See color version of this figure at back of this issue.

the DMSP (plot 3) and average ROCSAT-1 (plot 2) occurrence rates is 85%. Obvious discrepancies between the absolute values of the two occurrence rates reflect the different definitions applied for the two data sources. As indicated previously, because of its rapid precession, ROCSAT-1 spent significant time in the evening sector at latitudes far from the magnetic equator where it encountered no EPBs. The DMSP satellites used in this study always cross the magnetic equator in the part of the evening sector where EPBs are most apt to be observed. Second, at longitudes between the two vertical dashed lines (260°–320°) EPB occurrence rates measured by both DMSP and ROCSAT-1 show local minima. This longitude sector spans the eastern Pacific Ocean and the west coast of South America where B_{eq} approaches a global minimum.

[28] Embedded within the March and April occurrence rates shown in the middle plots of Figure 10 are seasonally/longitudinally dependent variations controlled by magnetic declination that changes from eastward to westward between 260° and 320°E. One way to eliminate seasonally dependent variations in order to identify purely longitudinal dependencies is to assign to each longitude bin its own maximum rate of occurrence ($\%_{max}$) as found in Figure 1. We assume that in the absence of a purely longitudinal dependence $\%_{max}$ would be approximately the same in all sectors. The bottom plot of Figure 10 shows $\%_{max}$ values measured by DMSP satellites between 1989 and 2002

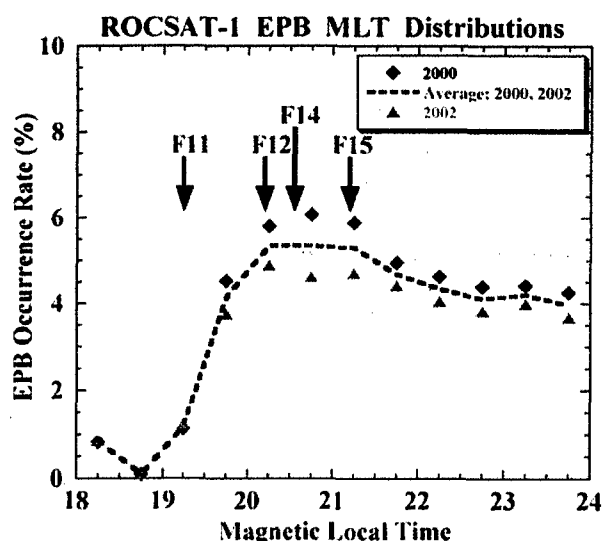


Figure 8. EPB occurrence rates for March and April 2000 (diamonds) and 2002 (triangles) plotted as a function of magnetic local time. The MLT of DMSP F11, F12, F14, and F15 orbital planes are indicated for reference.

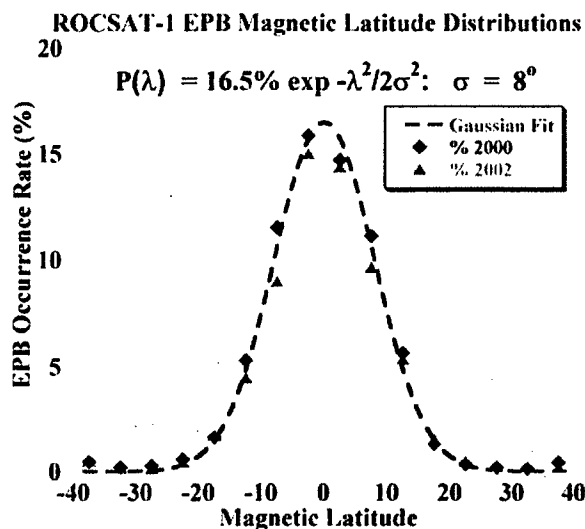


Figure 9. EPB occurrence rates for March and April 2000 (diamonds) and 2002 (triangles) plotted as a function of magnetic latitude. Gaussian fit to these data is provided as a guide for the eye.

[Burke *et al.*, 2004]. The $\%_{\max}$ distribution shows a steep gradient near 290°E rather than the minimum occurrence rate found in the March and April data.

[29] Figure 11 shows the latitudinal distribution of L-band scintillation activity observed by the South American GPS receiver chain in March and April 2002. Data are presented on an MLat versus day-of-month grid using a format described by Valladares *et al.* [2004b]. The color code uses red circles to indicate times when $S_4 > 0.5$ and blue dots to indicate times when scintillations were at background levels. Circles of other colors represent intermediate S_4 values. Horizontal black lines with open arrows indicate the highest magnetic latitudes where significant scintillation activity was detected on a given day. The top and bottom plots indicate the latitudinal breadths and intensities of scintillation activity observed by the GPS receivers when looking to the west and east, respectively. Two empirical aspects of these data should be noted. First, the GPS receivers were more likely to detect scintillations when looking to the east than to the west. This extends a similar result previously reported for August 2001 to February 2002 [Valladares *et al.*, 2004b]. Second, after 12 April 2002, scintillation activity vanished. This is a seasonal effect [Tsunoda, 1985] that is replicated in ROCSAT-1 measurements. Returning to the bottom plot of Figure 7, we see that after Julian day 102 of 2002 ROCSAT-1 detected no EPBs at longitudes between 280° and 300°E. The bottom plot of Figure 6 shows that EPB activity vanished within this longitude sector after Julian day 106 of 2000. For much of these intervals the ROCSAT-1 orbits were within 20° of the magnetic equator where it is most likely to encounter bubbles (Figure 10).

4. Discussion

[30] In the previous section we compared EPB observations by ROCSAT-1 and DMSP satellites in the evening

MLT sector. The comparison included individual bubbles detected near conjunctions. In the vast majority of cases when ROCSAT-1 detected a bubble, so did one or more DMSP satellites if their trajectories crossed at the same longitude within approximately ± 15 min. The only exceptions were bubbles observed by ROCSAT-1 very close to the magnetic equator that had not yet reached apex altitudes above 840 km. The F11 satellite with its orbital plane near the 1915 MLT meridian seldom detected bubbles in March and April 2000. Our survey suggests that ROCSAT-1 detected more EPBs at this MLT than did F11. This difference in observation frequency again appears related to the altitudes reached by EPBs shortly after sunset. Also, our statistical analysis showed that the rate of EPB encounters at topside altitudes rises rapidly between 1900 and 2000 MLT and peaks between 2000 and 2200 MLT (Figure 8). The fact that the orbital planes of F12, F14, and F15 lie in this MLT sector corroborates climatologies reported by Huang *et al.* [2001, 2002].

[31] The second significant result of our statistical analysis of the measurements involves near Gaussian EPB

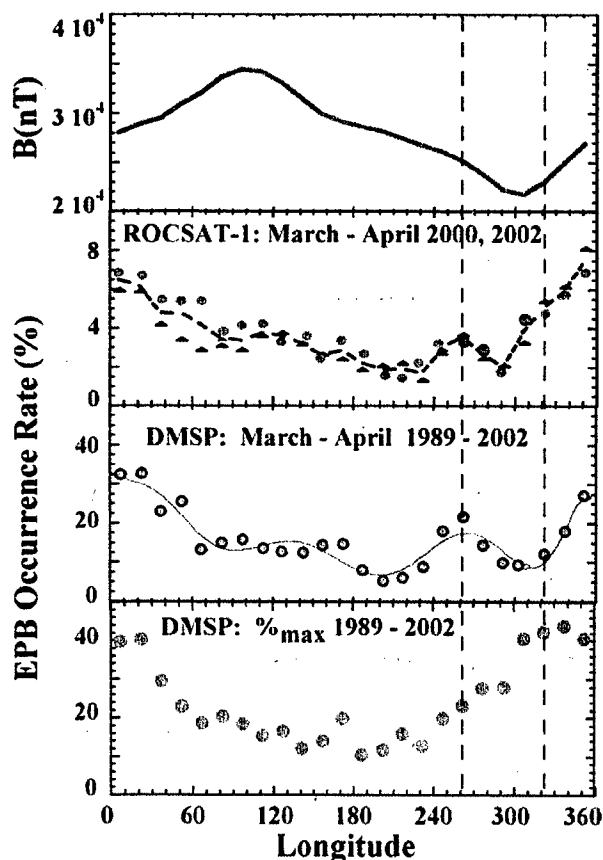


Figure 10. IGRF model values of the Earth's magnetic field strength B_{eq} at the magnetic equator at 350 km altitude (top). EPB occurrence rates observed in March and April 2000 and 2002 by ROCSAT-1 (second) and by DMSP satellites between 1989 and 2002 (third), and maximum occurrence rates $\%_{\max}$ observed by DMSP (bottom). All data are plotted as functions of geographic longitude.

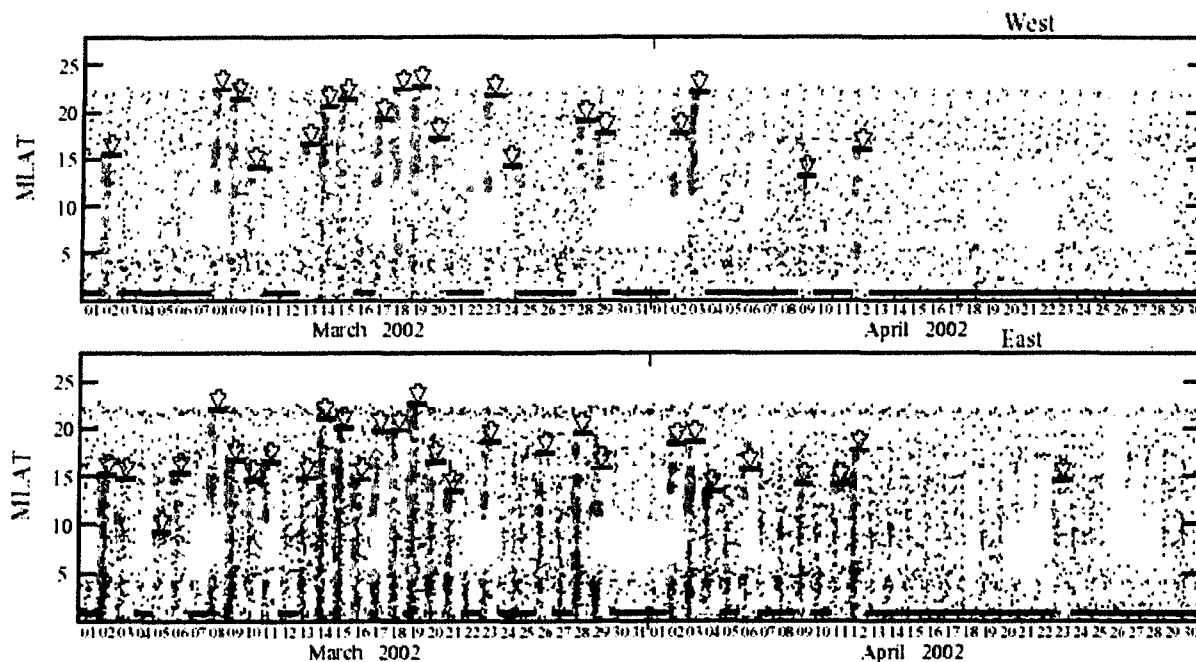


Figure 11. S4 index for L-band scintillations observed by the South American chain of GPS receivers plotted as magnetic latitude versus day-of-month for March and April 2002. Red circles indicate cases when $S4 > 0.5$. Horizontal black lines indicate the latitude ranges of severe scintillation activity. See color version of this figure at back of this issue.

distributions observed by ROCSAT-1 during both years. The parameter $\sigma \approx 8^\circ$ indicates that $>90\%$ of all EPBs were detected within $\pm 16^\circ$ of the magnetic equator (Figure 9). In the course of establishing the DMSP database, we examined $\sim 12,000$ orbits during which EPBs were detected. Although we did not record their magnetic latitudes for analysis, in the overwhelming majority of cases EPBs were detected at magnetic latitudes equatorward of $\pm 15^\circ$. At least qualitatively, this represents another point of substantial agreement between ROCSAT-1 and DMSP observations.

[32] Our comments on the longitudinal distribution of EPBs as observed with DMSP and ROCSAT-1 have two foci, their global distributions and the unexpectedly low occurrence rates in the South American sector. As mentioned previously, our motivation for initiating the present study was to establish limits of validity for DMSP-based global climatologies. Low occurrence rates, detected by both ROCSAT-1 and DMSP to the west of South America, suggest that forces previously unaccounted for act systematically at these longitudes to limit EPB occurrence. A review of geographical peculiarities of this sector is a necessary first step toward quantitative understanding of this phenomenon.

[33] Within the methodological constraints imposed by different orbital characteristics, EPB occurrence rates as a function of longitude appear to be quite similar at altitudes of 600 km (ROCSAT-1) and 840 km (DMSP). Although the comparison was done only for the months of March and April, these are close to the time when Tsunoda [1985] predicts near maximum occurrence rates at most longitudes and the Jicamarca radar detects the fastest upward drifts in the postsunset sector [Scherliess and Fejer, 1999]. The

result gives us confidence that the more general characteristics represented in Figure 1 and developed by Huang *et al.* [2002] are essentially correct. Also note that the observed similarities apply to the solar maximum conditions under which ROCSAT-1 data were acquired. Huang *et al.* [2002] found that EPBs seldom appear at 840 km during solar minimum. In some longitude sectors DMSP detected no EPBs during the solar minimum years 1996 and 1997. Approximately 40% of the EPBs DMSP encountered during these years are directly attributable to penetration electric field events. Thus the month versus longitude distribution in Figure 1 is heavily weighted by solar maximum observations. Whether ROCSAT-1 and DMSP will observe similar longitude distributions near solar minimum remains an open question.

[34] Seasonal/longitudinal variabilities in EPB occurrence rates are obvious in Figure 1. However, the very different ranges detected in the Atlantic-African versus Pacific sectors indicate purely longitudinal dependencies as well. Considerations of the $V_p = (\mathbf{E} \times \mathbf{B})/B^2$ term in the R-T growth rate equation led Huang *et al.* [2001] to suggest that the difference reflects equatorial magnetic field strengths characteristic of the different sectors. Figure 5 of Burke *et al.* [2004] plots $\%_{\max}$ as a function of B_{eq} . The data neatly break into two separate branches depending on whether B_{eq} increases or decreases with longitude. In both branches $\%_{\max}$ has relatively high values where B_{eq} is weak and low values where B_{eq} is strong. Both branches converge to about the same values in the high B_{eq} region. As can be seen in the bottom plot of Figure 10, $\%_{\max}$ is significantly higher to the east than to the west of 300°E where B_{eq} is minimal.

[35] In March and April both DMSP and ROCSAT-1 measurements show minima in occurrence rates near the west coast of South America. The chain of GPS receiver stations lies slightly eastward of the 290° meridian. Consistent with the ROCSAT-1 data, the GPS detectors observed decreasing rates of elevated S4 in March and April 2002. The off-equatorial stations also observed more scintillations coming from the east than from the west. This was true throughout the entire period from August 2001 through April 2002 as reported by *Valladares et al.* [2004a, 2004b], who demonstrated that enhanced S4 activity at off-equatorial stations coincides with topside plume activity detected by the Jicamarca Unattended Long-term studies of the Ionosphere and Atmosphere (JULIA) radar. The radar backscatter comes from meter-scale plasma-density irregularities collocated with EPBs [*Tsunoda et al.*, 1982]. We believe that empirical evidence for a steep gradient in EPB activity in the South American sector is compelling. The obvious question is, "Why is it there?"

[36] Two geographical features capable of influencing EPB formation occur at South American longitudes, the Andes Mountains and the South Atlantic Anomaly (SAA). *McClure et al.* [1998] suggested that wind turbulence above the Andes generates upward propagating gravity waves that seed bottomside density perturbations that grow into EPBs. For the sake of argument, let us grant that orogenic gravity waves favor EPB seeding in the South American sector. Indeed, gravity waves may well explain west-to-east gradients in $\%_{\max}$ and S4 enhancements near 300°E as reported by *Valladares et al.* [2004b]. However, this hypothesis explains neither the minimum out of which the gradient develops nor why high occurrence rates persist for thousands of kilometers to the east of the Andes.

[37] The SAA influences the R-T growth rate in two ways. Assuming that eastward electric fields in the evening sector are independent of longitude at the times of year when $\alpha = 0^\circ$, the $\mathbf{E} \times \mathbf{B}/B^2$ term indicates that growth is favored in regions of low B_{eq} . We note that near the west coast of South America eastward electric fields are greatest during March and April [*Scherliess and Fejer*, 1999] when the best alignment between the dusk terminator and equatorial magnetic field lines occurs (cf. Figure 1). A second possible contribution comes from the lead term $\Sigma_F/(\Sigma_F + \Sigma_E)$ in the R-T growth equation. This requires that the magnitude of Σ_E be significant.

[38] It is well known that radiation belt electrons (protons) in the drift loss cone precipitate to the west (east) of the minimum in B_{eq} . As they gradient-curvature drift around the Earth, trapped particles diffuse in pitch angle through particle-particle collisions and/or wave-particle interactions [*Blake et al.*, 2001]. As electrons drift eastward above the Pacific Ocean, their mirror altitudes in the Southern Hemisphere dip deeper and deeper into the upper atmosphere. Through collisions with ambient neutrals, they create ion-electron pairs in growing abundance as they approach the west coast of South America. Westward drifting ions are subject to similar effects while approaching the east coast of South America. The net effect is an increase in Σ_E near the SAA that does not occur at other longitudes. By itself, an increase in Pedersen conductance in the nightside E layer should diminish the growth rate of the R-T instability and

weaken the conductance gradient in Σ_P near the SAA. This in turn diminishes the polarization electric fields required for current continuity across the dusk terminator [*Eccles*, 1998a].

[39] Since energetic electrons are more efficient producers of ion-electron pairs and Pedersen conductance [*Galand and Richmond*, 2001], the effects of radiation belt precipitation should be more pronounced on the westward than the eastward side of the SAA. This effect is manifest in the lower EPB occurrence rates near the west coast of South America and the west to east gradient in S4 enhancements detected along the GPS receiver chain [*Valladares et al.*, 2004b]. Developing a detailed description of Σ_E profiles in the vicinity of the SAA goes well beyond the scope of this observational report. We believe that the experimental results presented here provide convincing evidence that precipitation from the radiation belt affects the global distribution of equatorial plasma bubbles and the climatology of radio wave scintillations. Quantification of this conclusion will depend on an integration of knowledge from scientists with both radiation belt and ionosphere/thermosphere expertise.

[40] **Acknowledgments.** The authors thank F. J. Rich of AFRL and J. M. Campbell of the Boston College Institute for Scientific Research for their generosity in making DMSP plasma data available. This work was supported under Air Force Office of Scientific Research task 2311SDA1, Air Force contract F19628-02-C-0012 with Boston College, and the National Polar-orbiting Operational Environmental Satellite System Internal Government Studies Program.

[41] Arthur Richmond thanks the reviewers for their assistance in evaluating this paper.

References

- Aarons, J. (1993), The longitudinal morphology of equatorial F layer irregularities relevant to their occurrence, *Space Sci. Rev.*, **63**, 209.
- Basu, B. (1997), Generalized Rayleigh-Taylor instability in the presence of time-dependent equilibrium, *J. Geophys. Res.*, **102**, 17,305.
- Basu, S., et al. (1996), Scintillations, plasma drifts and neutral winds in the equatorial ionosphere after sunset, *J. Geophys. Res.*, **101**, 26,795.
- Blake, J. B., U. S. Inan, M. Walt, T. F. Bell, J. Bortnik, D. L. Chenette, and H. J. Christian (2001), Lightning-induced energetic electron flux enhancements in the drift loss cone, *J. Geophys. Res.*, **106**, 29,733.
- Burke, W. J., C. Y. Huang, C. E. Valladares, J. S. Machuzak, L. C. Gentile, and P. J. Sultan (2003), Multipoint observations of equatorial plasma bubbles, *J. Geophys. Res.*, **108**(A5), 1221, doi:10.1029/2002JA009382.
- Burke, W. J., C. Y. Huang, L. C. Gentile, and L. Bauer (2004), Seasonal-longitudinal variability of equatorial plasma bubble occurrence, *Ann. Geophys.*, **22**, 3089.
- Chen, K. Y., H. C. Yeh, S. Y. Su, and C. H. Liu (2001), Anatomy of plasma structures in an equatorial spread F event, *Geophys. Res. Lett.*, **28**, 3107.
- Eccles, J. V. (1998a), A simple model of low-latitude electric fields, *J. Geophys. Res.*, **103**, 26,699.
- Eccles, J. V. (1998b), Modeling investigation of the evening prereversal enhancement of the zonal latitude electric field in the equatorial ionosphere, *J. Geophys. Res.*, **103**, 26,709.
- Fejer, B. G., and L. Scherliess (1997), Empirical models of storm time equatorial zonal electric fields, *J. Geophys. Res.*, **102**, 24,047.
- Fejer, B. G., E. R. de Paula, S. A. Gonzalez, and R. F. Woodman (1991), Average vertical and horizontal drifts at Jicamarca, *J. Geophys. Res.*, **96**, 13,901.
- Galand, M., and A. D. Richmond (2001), Ionospheric electrical conductances produced by auroral proton precipitation, *J. Geophys. Res.*, **106**, 117.
- Groves, K. M., et al. (1997), Equatorial scintillation and system support, *Radio Sci.*, **32**, 2047.
- Haerendel, G. (1973), Theory of equatorial spread F , report, Max Planck Inst. für Phys. und Astrophys. Res., Garching, Germany.
- Huang, C. Y., W. J. Burke, J. S. Machuzak, L. C. Gentile, and P. J. Sultan (2001), DMSP observations of equatorial plasma bubbles in the topside ionosphere near solar maximum, *J. Geophys. Res.*, **106**, 8131.
- Huang, C. Y., W. J. Burke, J. S. Machuzak, L. C. Gentile, and P. J. Sultan (2002), Equatorial plasma bubbles observed by DMSP satellites during a

- full solar cycle: Toward a global climatology, *J. Geophys. Res.*, 107(A12), 1434, doi:10.1029/2002JA009452.
- Hysell, D. L., M. C. Kelley, W. E. Swartz, and R. F. Woodman (1990), Seeding and layering of equatorial spread *F* by gravity waves, *J. Geophys. Res.*, 95, 17,253.
- Kil, H., and R. A. Heelis (1998), Global distribution of density irregularities in the equatorial ionosphere, *J. Geophys. Res.*, 103, 407.
- Luhmann, J. G., and A. L. Vampola (1977), Effects of localized sources on quiet time plasmasphere electron precipitation, *J. Geophys. Res.*, 82, 2671.
- McClure, J. P., S. Singh, D. K. Bamgboye, F. S. Johnson, and H. Kil (1998), Occurrence of equatorial *F* region irregularities: Evidence for tropospheric seeding, *J. Geophys. Res.*, 103, 29,119.
- Mendillo, M., J. Baumgardner, X. Pi, and P. J. Sultan (1992), Onset conditions for equatorial spread *F*, *J. Geophys. Res.*, 97, 13,865.
- Meriwether, J. W., J. L. Mirick, M. A. Biondi, F. A. Herrero, and C. G. Fesen (1996), Evidence for orographic wave heating in the equatorial thermosphere at solar maximum, *Geophys. Res. Lett.*, 23, 2177.
- Nopper, R. W., and R. L. Carovillano (1978), Polar-equatorial coupling during magnetically active periods, *Geophys. Res. Lett.*, 5, 699.
- Ott, E. (1978), Theory of Rayleigh-Taylor bubbles in the equatorial ionosphere, *J. Geophys. Res.*, 83, 2066.
- Pimenta, A. A., J. A. Bittencourt, P. R. Fagundes, Y. Sahai, R. A. Buriti, H. Takahashi, and M. J. Taylor (2003), Ionospheric plasma bubble zonal drifts over the tropical region: A study using OI 630 nm emission all-sky images, *J. Atmos. Sol. Terr. Phys.*, 65, 1117.
- Rich, F. J., and M. Hairston (1994), Large-scale convection patterns observed by DMSP, *J. Geophys. Res.*, 99, 3827.
- Scherliess, L., and B. G. Fejer (1999), Radar and satellite global equatorial *F* region vertical drift model, *J. Geophys. Res.*, 104, 6829.
- Singh, S., F. S. Johnson, and R. A. Power (1997), Gravity wave seeding of equatorial plasma bubbles, *J. Geophys. Res.*, 102, 7399.
- Stephan, A. W., M. Colerico, M. Mendillo, B. W. Reinisch, and D. Anderson (2002), Suppression of equatorial spread *F* by sporadic *E*, *J. Geophys. Res.*, 107(A2), 1021, doi:10.1029/2001JA000162.
- Sultan, P. J. (1996), Linear theory and modeling of the Rayleigh-Taylor instability leading to the occurrence of equatorial spread *F*, *J. Geophys. Res.*, 101, 26,875.
- Torr, D. G., M. R. Torr, J. C. G. Walker, and R. A. Hoffman (1975), Particle precipitation in the South Atlantic anomaly, *Planet. Space Sci.*, 23, 15.
- Tsunoda, R. T. (1985), Control of the seasonal and longitudinal occurrence of equatorial scintillations by the longitudinal gradient in the integrated *E*-region Pedersen conductivity, *J. Geophys. Res.*, 90, 447.
- Tsunoda, R. T., R. C. Livingston, J. P. McClure, and W. B. Hanson (1982), Equatorial plasma bubbles: Vertically elongated wedges from the bottom-side *F* layer, *J. Geophys. Res.*, 87, 9171.
- Valladares, C. E., J. Villalobos, R. Sheehan, and M. P. Hagan (2004a), Latitudinal extension of low latitude scintillations measured with a network of GPS receivers, *Ann. Geophys.*, 22, 3155.
- Valladares, C. E., R. Sheehan, and J. Villalobos (2004b), A latitudinal network of GPS receivers dedicated to studies of equatorial spread-*F*, *Radio Sci.*, 39, RS1S23, doi:10.1029/2002RS002853.
- Woodman, R. F., and C. LaHoz (1976), Radar observations of *F* region equatorial irregularities, *J. Geophys. Res.*, 81, 5447.
- Yeh, H. C., S. Y. Su, Y. C. Yeh, J. M. Wu, R. A. Heelis, and B. J. Holt (1999), Scientific mission of the IPEI payload onboard ROCSAT, *Terr. Atmos. Oceanic Sci.*, suppl., 19.
- Yeh, H. C., S. Y. Su, and R. A. Heelis (2001), Storm time plasma irregularities in the pre-dawn hours observed by the low-latitude ROCSAT satellite at 600 km altitude, *Geophys. Res. Lett.*, 28, 685.

W. J. Burke, Space Vehicles Directorate, Air Force Research Laboratory, 29 Randolph Road, Hanscom AFB, MA 01731-3010, USA. (william.burke2@hanscom.af.mil)

L. C. Gentile, C. Y. Huang, and C. E. Valladares, Institute for Scientific Research, Boston College, 402 St. Clement's Hall, 140 Commonwealth Avenue, Chestnut Hill, MA 02467-3862, USA. (louise.gentile@hanscom.af.mil; cheryl.huang@hanscom.af.mil; valladar@bc.edu)

S. Y. Su, Institute of Space Science and Center for Space and Remote Sensing Research, National Central University, Chung-Li 32054, Taiwan. (sysu@jupiter.ss.ncu.edu.tw)

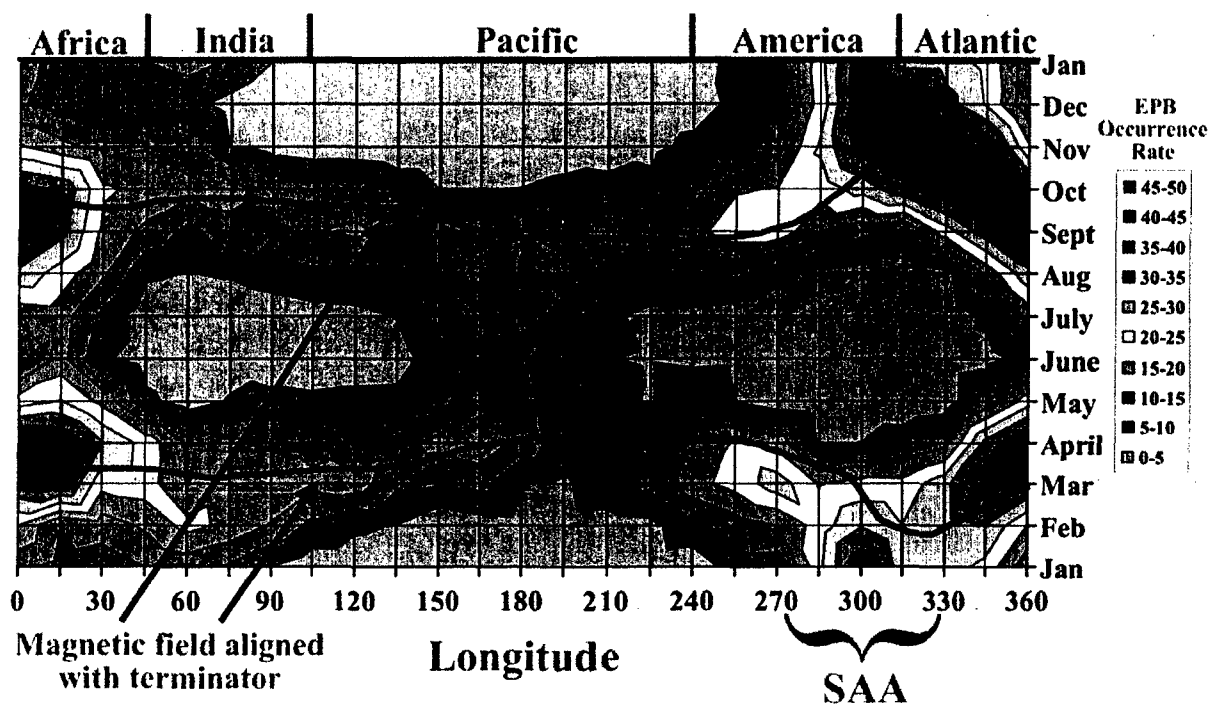


Figure 1. Contours of equatorial plasma bubble (EPB) occurrence rates measured by DMSP satellites between 1989 and 2002 plotted on a month versus longitude grid in nine 5% increments. The solid lines indicate the two times per year when $\alpha = 0^\circ$ at given longitudes.

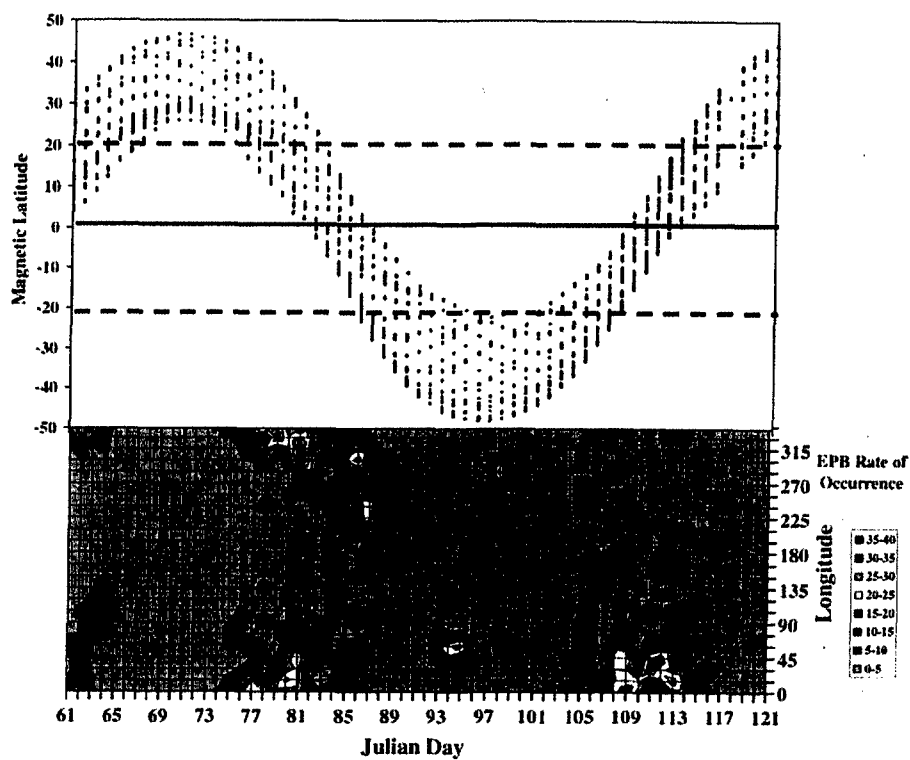


Figure 6. Magnetic latitudes of ROCSAT-1 at 2100 MLT (top) and contours of EPB occurrence rates plotted on a longitude versus Julian day grid (bottom) for 1 March to 30 April 2000.

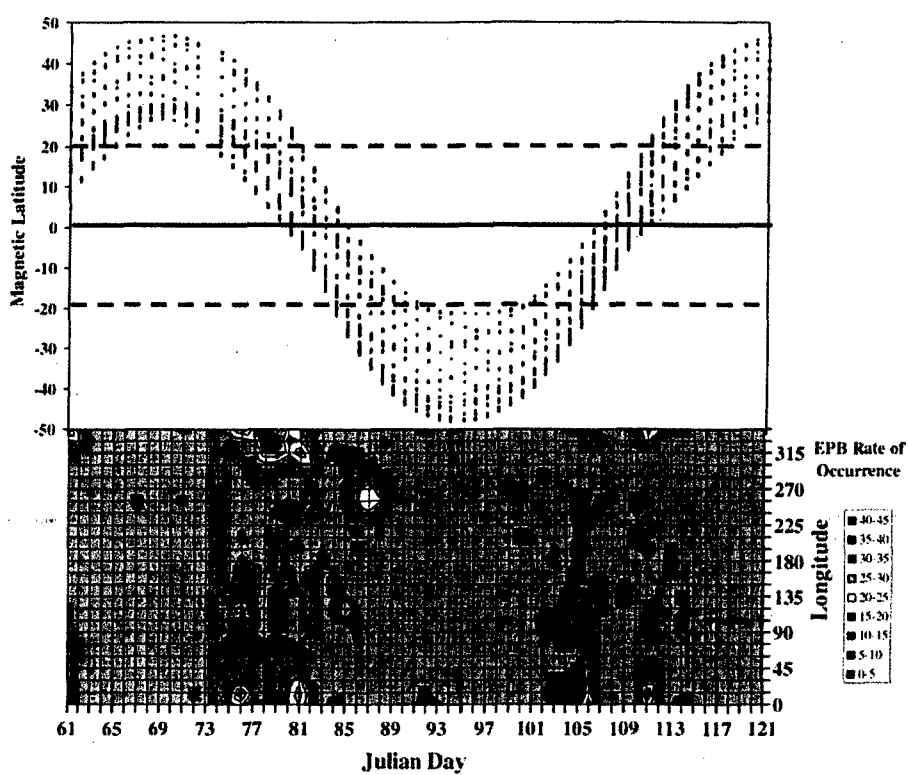


Figure 7. Magnetic latitudes of ROCSAT-1 at 2100 MLT (top) and contours of EPB occurrence rates plotted on a longitude versus Julian day grid (bottom) for 1 March to 30 April 2002.

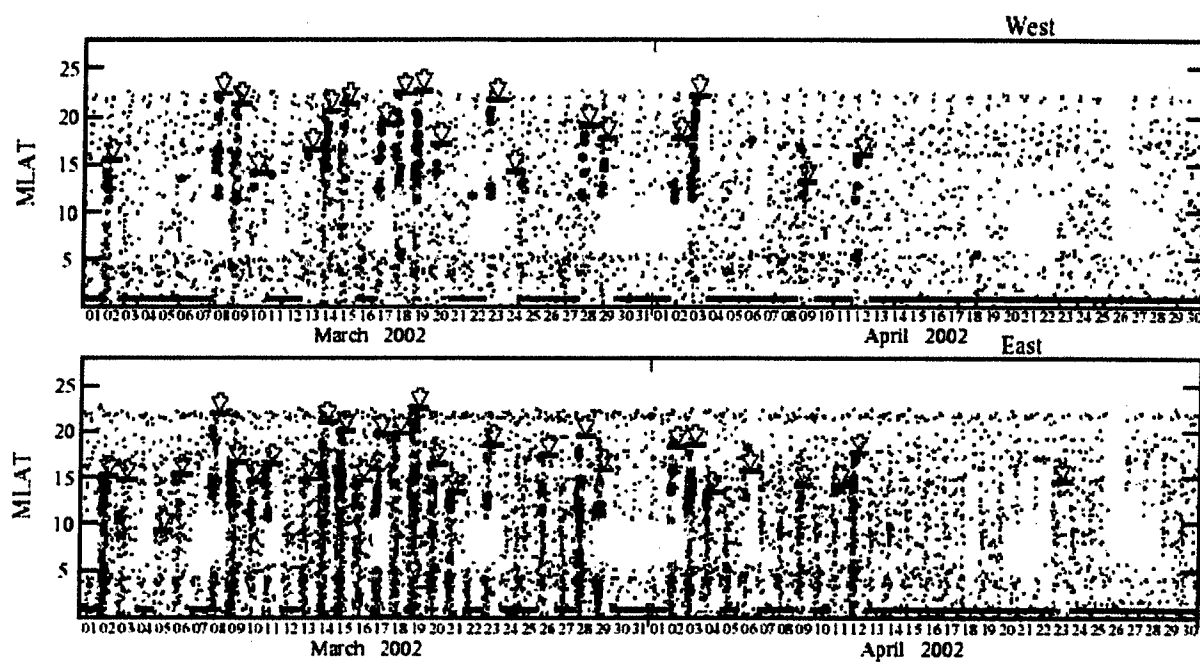


Figure 11. S4 index for L-band scintillations observed by the South American chain of GPS receivers plotted as magnetic latitude versus day-of-month for March and April 2002. Red circles indicate cases when $S4 > 0.5$. Horizontal black lines indicate the latitude ranges of severe scintillation activity.

REPORT DOCUMENTATION PAGEForm Approved
OMB No. 0704-0188

Public reporting burden for this collection of information is estimated to average 1 hour per response, including the time for reviewing instructions, searching existing data sources, gathering and maintaining the data needed, and completing and reviewing this collection of information. Send comments regarding this burden estimate or any other aspect of this collection of information, including suggestions for reducing this burden to Department of Defense, Washington Headquarters Services, Directorate for Information Operations and Reports (0704-0188), 1215 Jefferson Davis Highway, Suite 1204, Arlington, VA 22202-4302. Respondents should be aware that notwithstanding any other provision of law, no person shall be subject to any penalty for failing to comply with a collection of information if it does not display a currently valid OMB control number. PLEASE DO NOT RETURN YOUR FORM TO THE ABOVE ADDRESS.

1. REPORT DATE (DD-MM-YYYY)

13-06-2005

REPRINT

4. TITLE AND SUBTITLELongitudinal Variability of Equatorial Plasma Bubbles Observed
by DMSP and ROCSAT-1**5a. CONTRACT NUMBER****5b. GRANT NUMBER****5c. PROGRAM ELEMENT NUMBER**
61102F**6. AUTHOR(S)**W.J. Burke, L.C. Gentile*, C.Y. Huang*, C.E. Valladares*,
S. Y. Su****5d. PROJECT NUMBER**
2311**5e. TASK NUMBER**
SD**5f. WORK UNIT NUMBER**
A3**7. PERFORMING ORGANIZATION NAME(S) AND ADDRESS(ES)**Air Force Research Laboratory/VSBXP
29 Randolph Road
Hanscom AFB MA 01731-3010**8. PERFORMING ORGANIZATION REPORT
NUMBER**

AFRL-VS-HA-TR-2005-1059

9. SPONSORING / MONITORING AGENCY NAME(S) AND ADDRESS(ES)**10. SPONSOR/MONITOR'S ACRONYM(S)****11. SPONSOR/MONITOR'S REPORT
NUMBER(S)****12. DISTRIBUTION / AVAILABILITY STATEMENT**

Approved for Public Release; Distribution Unlimited.

*Institute for Scientific Research, Boston College, Chestnut Hill, MA

**Institute of Space Science, National Central Univ, Chung-Li, Taiwan

13. SUPPLEMENTARY NOTESREPRINTED FROM: JOURNAL OF GEOPHYSICAL RESEARCH, Vol 109, A12301
doi: 10.1029/2004JA010583, 2004.**14. ABSTRACT**

[1] We compare observations of equatorial plasma bubbles (EPBs) by polar-orbiting satellites of the Defense Meteorological Satellite Program (DMSP) with plasma density measurements from the Republic of China Satellite (ROCSAT-1) in a low-inclination orbit. DMSP data were acquired in the evening sector at low magnetic latitudes between 1989 and 2002. ROCSAT-1 plasma densities were measured in March and April of 2000 and 2002. Observations of individual EPBs detected by both ROCSAT-1 and DMSP were well correlated when satellite orbital paths crossed the same longitude within approximately ± 15 min. We compiled a statistical database of ROCSAT-1 EPB occurrence rates sorted by magnetic local time (MLT), magnetic latitude, and geographic longitude. The rate of ROCSAT-1 EPB encounters at topside altitudes rose rapidly after 1930 MLT and peaked between 2000 and 2200 MLT, close to the orbital planes of DMSP F12, F14, and F15. EPB encounter rates have Gaussian distributions centered on the magnetic equator with half widths of $\sim 8^\circ$.

15. SUBJECT TERMSEquatorial plasma bubbles
Magnetic latitudesDMSP
ROCSAT-1
Ionospheric scintillations**16. SECURITY CLASSIFICATION OF:****a. REPORT**
UNCLAS

UNCLAS

c. THIS PAGE
UNCLAS**17. LIMITATION
OF ABSTRACT**

SAR

**18. NUMBER
OF PAGES****19a. NAME OF RESPONSIBLE PERSON**
W. Burke**19b. TELEPHONE NUMBER (include area
code)**
781-377-3980